Experimental/Numerical Investigation of the Influence of a Pressure Gradient on Acoustic Roughness Receptivity in the Boundary Layer of a 2-D Airfoil

S. Herr, A. Wörner, W. Würz, U. Rist, S. Wagner
Universität Stuttgart, Institut für Aerodynamik und Gasdynamik
Pfaffenwaldring 21, D-70550 Stuttgart, Germany

Summary

In the present paper, the influence of a pressure gradient on the acoustic roughness receptivity is investigated by means of wind tunnel experiments and Direct Numerical Simulations (DNS). The receptivity function for three different locations of a 3-D surface non-uniformity on a 2-D airfoil is calculated from the experimental and numerical data and compared to each other. The combined effects of the roughness acoustic receptivity and the amplification of the generated disturbances are taken into account in order to evaluate the position on the airfoil at which a surface non-uniformity is most dangerous in provoking an early transition.

Introduction

The problem of the boundary layer transition from laminar to turbulent flow still attracts much attention because of its fundamental and practical importance. It has three main parts. First, there is the laminar flow receptivity to external (acoustic or vortical) perturbations. The second part is the region where the boundary layer instabilities develop according to linear stability theory. And finally, there is the nonlinear flow breakdown to turbulence. This paper is devoted to experimental and numerical investigations of the linear 3-D acoustic receptivity of a 2-D laminar boundary layer in the presence of a localized (3D) quasi steady surface non-uniformity. Pressure gradients strongly influence the amplification of disturbances in a transitional boundary layer. The location of transition is not only determined by the amplification of the disturbances, but also by their initial amplitude. As the initial amplitude itself is determined by the process of receptivity, it should be of interest whether a large scale pressure gradient may have an influence on the receptivity of a boundary layer to freestream perturbations.

This problem has been poorly studied so far. Most studies consider a Blasius flow as base flow [8], [6]. The 3-D vibrational receptivity of a 2-D self-similar boundary layer with an adverse pressure gradient was investigated experimentally in [5], and recently the influence of a favorable pressure gradient was studied in [4]. A numerical investigation on the influence of the pressure gradient on boundary layer receptivity can be found in [1]. In the present study, we would like to determine the role a large scale pressure gradient plays with regard to the acoustic receptivity of a boundary layer in the presence of a small scale surface non-uniformity on an airfoil.

In an earlier experiment and accompanying DNS, the acoustic receptivity function of a 3-D roughness element on an airfoil was determined quantitatively [13]. The receptivity function was defined as the ratio of the initial (i.e. at the surface non-uniformity) amplitude of the instability wave, generated in the boundary layer, to the amplitude of the external acoustic perturbation and the amplitude of the corresponding (localized) surface non-uniformity

$$\widetilde{G}_{av}(\alpha,\beta) = \frac{\widetilde{B}_{inTS}(\alpha,\beta)}{\widetilde{A}_{ac} \cdot \widetilde{A}_{v}(\alpha,\beta)}$$

for every spanwise and streamwise wave number of the developing TS-wave train as proposed in [3]. The surface roughness was located at the point of neutral stability of branch I for the investigated frequency (1088 Hz). It is located at $\frac{s}{s_{max}} = 20\%$ on the symmetrical airfoil (XIS40MOD) [11], figure 1. The boundary layer profile at this position ($H_{12} = 2.58$) is close to that of the Blasius boundary layer figure 2, and therefore the accompanying DNS could be performed for the Blasius flow [9].

In a preliminary investigation, two additional positions were chosen for the present study. The position $\frac{s}{s_{max}} = 15\%$ corresponds to a favorable pressure gradient (figure 1). The position $\frac{s}{s_{max}} = 30\%$ lies in the region of the instability ramp of the airfoil figure 1. DNS were performed for Falkner-Skan self-similar boundary layers. For the position $\frac{s}{s_{max}} = 30\%$ a Falkner-Skan profile with Hartree parameter $\beta_H = -0.05$ was used and for position $\frac{s}{s_{max}} = 15\%$ a Hartree parameter $\beta_H = 0.05$ was used see figure 2.

Numerical Approach

The DNS are based on the velocity-vorticity formulation of the complete Navier-Stokes equations for incompressible fluids.

$$\frac{\partial \omega}{\partial t} - \mathrm{rot}\,(\underline{v} \times \underline{\omega}) = \frac{1}{Re}\,\Delta\underline{\omega}$$
$$\text{with} \quad \underline{v} = (u,v,w) \quad \text{and} \quad \underline{\omega} = (\omega_x,\omega_y,\omega_z)$$

All lengths are non-dimensionalized using a reference length $\tilde{L}$ and all velocities using the freestream velocity $\tilde{U}_\infty$ at the inflow boundary, where $\tilde{}$ denotes dimensional variables. A sketch of the integration domain is shown in figure 3. The flowfield is discretized using fourth-order accurate finite differences in streamwise (x-) and wall-normal (y-) direction, and a spectral method in spanwise (z-) direction. The time integration is done using a fourth order, four step Runge-Kutta scheme. Details concerning the numerical method can be found in [7].

A pressure gradient is imposed on the boundary layer by prescribing the streamwise velocity at the upper boundary of the integration domain. For the study shown here, this is done using the Falkner-Skan ansatz for self similar boundary layers. This means that the streamwise velocity at the upper boundary u_e is set to:

$$u_e(x) = u_0 \cdot x^m, \quad \text{with} \quad m = \frac{\beta_H}{(2-\beta_H)}$$

If $\beta_H < 0$ the flow is decelerated, which means that an adverse pressure gradient is imposed, whereas for $\beta_H > 0$ the flow is accelerated or a favorable pressure gradient is imposed.

The sound wave is modelled using the analytical solution of the second Stokes' problem. This solution is added to the steady Falkner-Skan or, at zero pressure gradient, Blasius velocity profile, which is prescribed at inflow. The small roughness element within the equidistant cartesian grid is modelled by extrapolating the velocity at the lowest row of grid points in such a way as to fulfil the no-slip and the non-permeability condition at the surface of the roughness. This is done using fifth order polynomials in $y-$direction which are consistent to the finite difference representation of the flowfield.

In contrast to the experiments, the interaction of a planar sound wave with a roughness element of one discrete spanwise wave number is calculated, and the complex receptivity function is evaluated for every spanwise wave number separately. For the 2-D case, the evaluation of the receptivity function requires four numerical simulations. In the first simulation the steady flow over a flat plate with a roughness element located at a certain distance from the leading edge is calculated using the unsteady Navier-Stokes equations starting with the flow over a flat plate without roughness. In the second simulation, the interaction of the sound wave with the roughness is calculated using the previously calculated steady flow as initial condition. The difficulty now is to extract the Tollmien-Schlichting(TS) wave, which is created by the interaction of the sound wave with the roughness, from the total solution. There are two problems. The first one is that the sound wave itself has the same frequency as the created TS-wave, and the second is that there is a numerically created TS-wave resulting from an approximate inflow condition. These problems are solved using a method suggested by Crouch & Spalart [2]. Therefore, a third simulation is needed including the sound wave but no roughness. In this simulation the TS-wave created at the inflow boundary is also present. So the TS-wave created at the roughness can be extracted from the total solution by subtracting the results of the third simulation from the results of the second one. Next, a Fourier analysis is used to determine the amplitude and phase part of the TS-wave at every streamwise position. The 'theoretical' amplitude of the TS-wave at the center of the roughness element is found by matching the amplitudes of the TS-wave created by the interaction with the amplitudes of a TS-wave created in a fourth simulation (the so called reference simulation) by blowing and suction at the wall upstream of the roughness element. This can be seen in figure 5, where the amplification curve of a TS-wave which is created by the interaction of a sound wave with a surface non-uniformity located at $Re_{\delta_1} = 1205$ within an adverse pressure gradient region is shown together with its reference simulation. For the 3-D case, the third simulation is not necessary because the TS-wave can be distinguished from the sound wave and the numerical TS-wave because of its different spanwise wave number.

Experimental Approach

The hot-wire measurements were carried out in the Laminar Wind Tunnel of the *Institut für Aerodynamik und Gasdynamik* [10]. The high contraction ratio of 100:1, as well as five screens and filters, result in a very low turbulence level of less than $2 \cdot 10^{-4}$. Downstream of the airfoil model a loudspeaker was mounted in a streamline shaped housing to insert the sound wave with a frequency $f_{ac} = 1088Hz$ as external perturbation. This sound wave had a sound pressure level of approximately $100dB$ in the test section, that is $16dB$ higher than the natural sound pressure level for the frequency range $10Hz - 5000Hz$ of the wind tunnel itself.

The roughness was modelled by the deflection of the membrane of a vibrating source [12]. The active diameter $(6mm)$ was chosen to be approximately one half of the TS-wavelength (at f_{ac}) to allow a significant amount of amplitude at higher spanwise wave numbers. The membrane is vibrating with a very low frequency compared to the acoustic frequency $f_v : f_{ac} = 1 : 64$. This leads to an amplitude modulation of the resulting TS-wave, which is visible in the spectrum as discrete sidepeaks at frequencies $f_{TS1,2} = f_{ac} \mp f_v$. The TS-waves at these combination frequencies result from the scattering of the sound on the surface vibrator only. They are separated from the TS-amplitude at f_{ac} which is contaminated by signals from different sources (acoustic, probe vibration etc.). On the other hand, the ratio between the acoustic frequency and the frequency of the surface vibrations is big enough that the roughness can be assumed quasi stationary and the resulting receptivity function can be compared to DNS for stationary roughness. The shape

of the membrane was measured and double Fourier transformed in streamwise and spanwise direction in order to determine the complex wave number spectrum of the surface vibration at the vibrational frequency:

$$\widetilde{A}_v(\alpha,\beta) = \int_{-\infty}^{\infty}\int_{-\infty}^{\infty} \widetilde{A}_m(s,z)\cdot e^{-i(\alpha s+\beta z)} ds\, dz\,.$$

Therefore, the resulting receptivity function is independent of the actual shape of the roughness. The ratios between the frequencies were chosen as integer powers of two ($f_v : f_{ac} : f_{samplerate} = 1:64:8$) and the frequencies were strictly phase locked because they were subdivided from a single quartz based clock. Therefore it was possible to use both the amplitude and the phase part of the Fast Fourier Transform of the hot-wire signal for further data processing. The measurement procedure was controlled by a PC and the results were monitored online. The complete setup is sketched in figure 4. Details on the setup, the measurement procedure and data evaluation can be found in [12].

Two main sets of data were collected, consisting of 13 respectively 5 scans in spanwise direction which covered the whole width of the TS-wave train developing downstream of the roughness. The time signals at every measurement point were analyzed with a FFT and the complex amplitude

$$\widetilde{A}_{TS,1/2,raw}(s_i,z) = A_{TS,1/2,raw}(s_i,z)\cdot e^{i\phi_{TS,1/2}(s_i,z)}$$

formed by the amplitude part ($A_{TS,1/2,raw}$) and the phase part ($\phi_{TS,1/2}$) for the combination frequencies was used for further processing. The amplitudes were normalized by the local freestream velocity U_δ. The phases were corrected in streamwise and spanwise direction by adding multiples of 360^o. The wave train at the right combination frequency developing downstream of the source at $\frac{s}{s_{max}} = 15\%$ is plotted in figures 7 and 8. The complex values of the wave train in physical space were mapped for each spanwise cut to wave number spectra by the complex Fourier transform

$$\widetilde{B}_{TS}(s_i,\beta) = \int_{-\infty}^{\infty} \widetilde{A}_{TS}(s_i,z)\cdot e^{-i\beta z} dz\,.$$

After this decomposition, the downstream development of waves with different spanwise wave numbers can be followed separately.

Similar to the procedure used in the DNS the initial amplitude at the position of the roughness is found by comparison to a reference amplification curve. The reference in the experimental case is the amplification as it is predicted by the linear stability theory. This is sketched in figure 6 for the wave number $\beta = \pm 0.269\frac{1}{mm}$ and the roughness located at $\frac{s}{s_{max}} = 15\%$. In the same figure, the phase part for the same wave number is plotted. The phases for all wave numbers can be interpolated by a straight line. The gradient of this line corresponds to the streamwise wave number α_r of the TS-wave. As a result, a dependence of α_r on β can be obtained which is called the dispersion dependence. The propagation angle can be found as $\theta = \arctan\frac{\beta}{\alpha_r}$. From the double Fourier decomposition of the shape of the membrane, the vibrational amplitudes that generate eigenmodes of the boundary layer can be found along the dispersion function.

Results

The receptivity function as a function of the propagation angle θ is shown in figure 9 for the three investigated streamwise positions of the roughness element. The big symbols mark the

results of the DNS which are in excellent agreement with the experimental results. The velocity fluctuations (B_{inTS}, A_{ac}) are normalized with the freestream velocity U_δ at the position of the roughness, and all linear dimensions (A_v, dz, ds) are normalized with the displacement thickness δ_1 of the boundary layer at the position of the roughness element which is indicated in figure 9. As a result of this normalization, the receptivity function depends on a local value of the boundary layer, the displacement thickness δ_1. In order to be able to study exclusively the dependence of the acoustic receptivity on the external pressure gradient, DNS were performed where all other parameters, particularly the Reynolds number Re_{δ_1}, based on the boundary layer displacement thickness, were kept constant at the location of the surface non-uniformity.

In figure 10 the receptivity function G_{av} for a 2-D roughness element located at $Re_{\delta_1} = 1205$ is plotted versus the wall shear stress, which is non-dimensionalized by the freestream velocity and the displacement thickness at the location of the roughness element. It can be seen that for the cases studied the acoustic receptivity depends only weakly on the external pressure gradient. The wall shear stress at the roughness lies between $0.54 - 0.62$ which leads to a change in the receptivity coefficient of about 15%. Similar to the results for vibrational receptivity, a favorable pressure gradient leads to an increase in the acoustic receptivity whereas an adverse pressure gradient reduces it. This means that the acoustic receptivity behaves in reverse to the instability which is decreased by a favorable pressure gradient and increased by an adverse one. This can be explained as follows: The wall shear stress $\frac{dU}{dy}$ is a function of the Hartree parameter β_H and increases if the flow is decelerated. The roughness enters the receptivity mainly by the fact that the steady part of the streamwise velocity U at the lowest row of grid points scales with $h \cdot \frac{dU}{dy}$ (see also [1]). So this is the reason why the receptivity function for a roughness located at a fixed Re_{δ_1} scales with the local wall shear stress.

For practical application, it is of great interest to find the position on the airfoil where a roughness with constant height results in the highest TS-amplitudes far downstream. If we assume a disturbance with $A_{ac} \cdot A_v = \frac{1}{\delta_1}$ constant for every propagation angle θ, we find the initial TS-amplitudes as $B_{inTS} = G_{av} \cdot A_{ac} A_v$. We consider a control position far downstream of the roughness at $\frac{s}{s_{max}} = 45.2\%$. The N-factor from the roughness position to this control position, N_c, can be found in figure 1, and the amplitudes at the control position $B_{TS,45.2\%} = B_{inTS} \cdot e^{N_c}$ are plotted in figure 11. The relation between these amplitudes reflects the relation of the amplitudes resulting from a roughness of constant dimensional height placed at different streamwise positions close to the instability point of the airfoil. Figure 11 shows that a roughness element placed at branch I of the neutral stability curve ($\frac{s}{s_{max}} = 20\%$) leads to earliest transition.

Conclusion

We have shown experimental as well as numerical results concerning the influence of a pressure gradient on the acoustic roughness receptivity in the boundary layer of a 2-D airfoil. The receptivity functions evaluated experimentally for three different positions of the surface non-uniformity on the airfoil and numerically for *Falkner-Skan* flows with three different Hartree parameters agreed very well. The values of the receptivity function didn't change much when the position of the surface non-uniformity on the airfoil was varied. This is also due to the fact that the receptivity function as it is defined here depends on the length scale that is used for non-dimensionalization. Since here the local displacement thickness at the location of the roughness was chosen, the influence of the pressure gradient on the receptivity could not be completely separated from the influence of the growth of the boundary layer.

Therefore, DNS were performed where Re_{δ_1} at the location of the roughness as well as the dimensionless frequency F were kept constant so that we were able to study only the influence of the pressure gradient. This study showed that a favorable pressure gradient increases the acoustic roughness receptivity whereas an adverse pressure gradient slightly reduces it, which is in accordance with increased and decreased wall shear stress, respectively. This influence is contrary to the influence of the pressure gradient on the instability of the boundary layer. If we take into account that a combination of both effects determines the amplitude of the boundary layer disturbances far downstream, it turns out that the influence of the pressure gradient on the acoustic roughness receptivity is much weaker than its influence on the boundary layer stability. Therefore the most dangerous position for a surface non-uniformity on an airfoil with respect to transition is the location of branch I of the neutral stability curve.

Acknowledgement

This work was performed under grant of the German research council (DFG) and is a contribution to the research program 'Transition'.

References

[1] Choudhari M., Lian N., Street C.L.: *Acoustic receptivity due to weak surface inhomogeneities in adverse pressure gradient boundary layers*; NASA Technical Memorandum 4577, 1995

[2] Crouch J.D., Spalart P.R.: *A study of non-parallel and nonlinear effects on the localized receptivity of boundary layers*; J. Fluid Mech., pp. 29-37, Vol. 290, 1995

[3] Gaster M., Grant I.: *An experimental investigation of the formation and development of a wave packet in a laminar boundary layer*; Proc. R. Soc. of London A; 347, pp. 253-269, 1975

[4] Ivanov A.V., Kachanov Y.S., Bake S., Neemann K.: *Influence of favorable pressure gradient on 3-D vibrational receptivity of boundary layer*; ICMAR Proc. Part 2, ITAM, Novosibirsk, pp. 78-83, 2000

[5] Kachanov Y.S., Koptsev D.B., Smorodskiy B.V.:*3-D stability and receptivity of two-dimensional self-similar boundary layer with adverse pressure gradient*; Laminar-Turbulent Transition, Proceedings IUTAM Symposium, Eds. Fasel H., Saric W., Berlin Springer-Verlag 1999

[6] Kosorygin V.S., Radetztsky R.H., Saric W.S.: *Laminar boundary layer sound receptivity and control*; Laminar-Turbulent Transition Vol. IV, Ed. Kobayashi R., Springer 1995

[7] Rist U., Fasel H.: *Direct numerical simulation of controlled transition in a flat-plate boundary layer* J. Fluid Mech., pp. 211-248, Vol. 298, 1995

[8] Saric W.S., Radetzky J.A., Hoos R.H. jr: *Boundary layer receptivity of sound with roughness*; Boundary Layer Stability and Transition, FED-Vol. 114, Eds. Reda, Reed, Kobayashi, ASME, 1991

[9] Wörner A., Rist U., Herr S., Würz W., Wagner S., Kachanov Y.S.: *Study of the acoustic receptivity of a Blasius boundary layer in the presence of a surface non-uniformity*; ECCOMAS 2000, Barcelona 11.-14.9.2000

[10] Wortmann F.X., Althaus D.: *Der Laminarwindkanal des Instituts für Aerodynamik und Gasdynamik der Technischen Hochschule Stuttgart*;Zeitschrift für Flugwissenschaften Nr.12 Heft 4, 1964

[11] Würz W.: *Hitzdrahtmessungen zum laminar-turbulenten Strömungsumschlag in anliegenden Grenzschichten und Ablöseblasen sowie Vergleich mit der linearen Stabilitätstheorie und empirischen Umschlagskriterien*; Dissertation, Universität Stuttgart, 1995

[12] Würz W., Herr S., Wagner S., Kachanov Y.S.: *Experimental investigation on 3-D acoustic receptivity of a laminar boundary layer in the presence of surface non-uniformities*; New Results in Numerical and Experimental FLuid Mechanics 2, Eds. Nitsche W., Heinemann H.-J., Hilbig R., Vieweg 1999

[13] Würz W., Herr S., Wörner A., Rist U., Wagner S., Kachanov Y.S.: *Study of 3-D wall roughness acoustic receptivity on an airfoil*; Laminar-Turbulent Transition, Proceedings IUTAM Symposium, Eds. Fasel H., Saric W., Berlin Springer-Verlag 1999

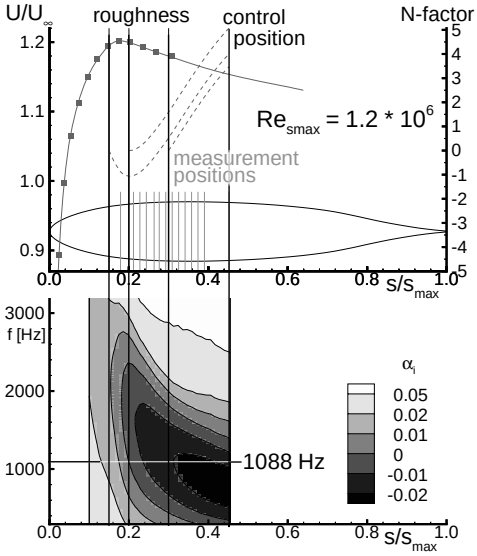

Figure: 1 Velocity distribution and position of the roughness in stability diagram

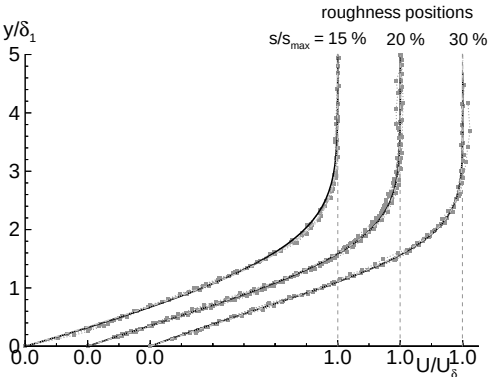

Figure: 2 Boundary layer profiles at the chosen streamwise positions of the roughness

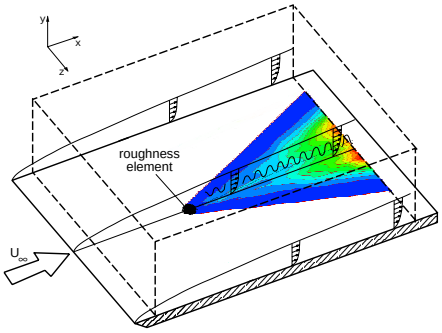

Figure: 3 Integration domain for the DNS

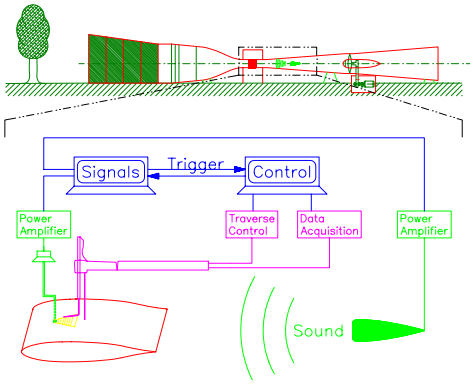

Figure: 4 Experimental setup at the Laminar Wind Tunnel

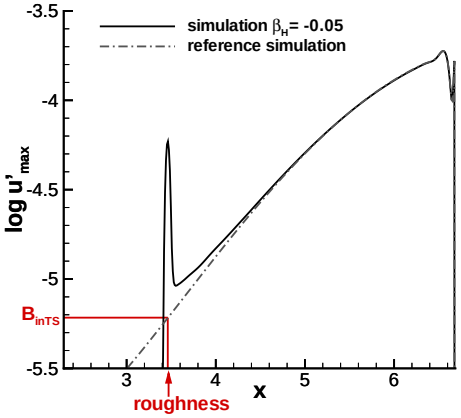

Figure: 5 Amplification as calculated by DNS

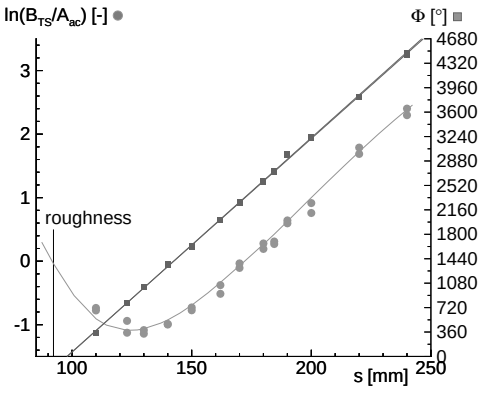

Figure: 6 Downstream development of amplitude and phase for $\beta = 0.269\frac{1}{mm}, \theta = 25^o$

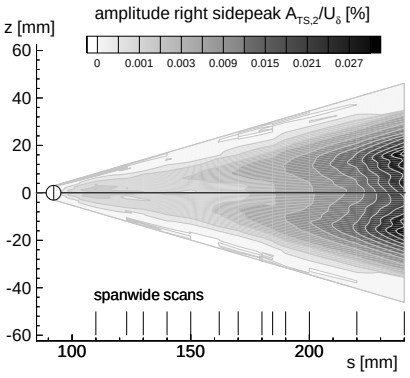

Figure: 7 Amplitude part of the wave train roughness at $\frac{s}{s_{max}} = 15\%$

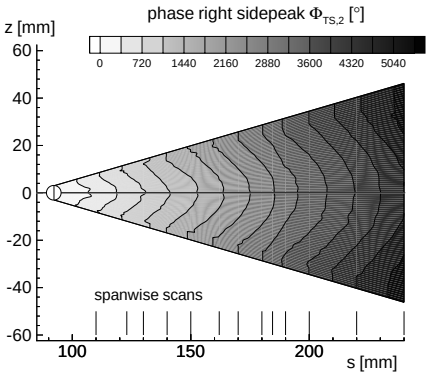

Figure: 8 Phase part of the wave train roughness at $\frac{s}{s_{max}} = 15\%$

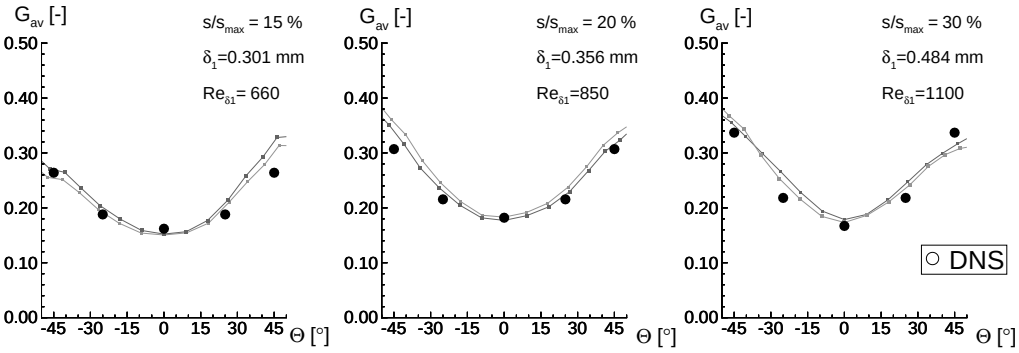

Figure: 9 Receptivity function for roughness at different streamwise positions

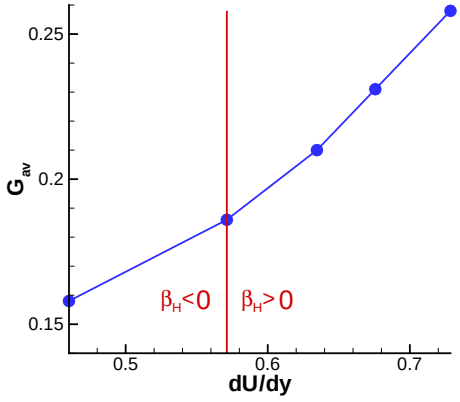

Figure: 10 Receptivity function for different Hartree parameters β_H

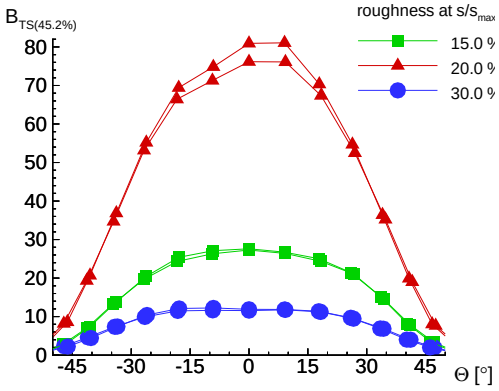

Figure: 11 TS-amplitudes at control position for roughness at different streamwise positions